Digital memory device based on tobacco mosaic virus conjugated with nanoparticles

RICKY J. TSENG[1]*, CHUNGLIN TSAI[2]*, LIPING MA[1], JIANYONG OUYANG[1], CENGIZ S. OZKAN[3†] AND YANG YANG[1†]

[1]Department of Materials Science and Engineering, University of California–Los Angeles, Los Angeles, California 90095, USA
[2]Department of Electrical Engineering, University of California–Riverside, Riverside, California 92521, USA
[3]Department of Mechanical Engineering, University of California–Riverside, Riverside, California 92521, USA
*These authors contributed equally to this work.
†e-mail: yangy@ucla.edu; cozkan@engr.ucr.edu

Published online: 4 October 2006; doi:10.1038/nnano.2006.55

Nanostructured viruses are attractive for use as templates for ordering quantum dots to make self-assembled building blocks for next-generation electronic devices. So far, only a few types of electronic devices have been fabricated from biomolecules due to the lack of charge transport through biomolecular junctions. Here, we show a novel electronic memory effect by incorporating platinum nanoparticles into tobacco mosaic virus. The memory effect is based on conductance switching, which leads to the occurrence of bistable states with an on/off ratio larger than three orders of magnitude. The mechanism of this process is attributed to charge trapping in the nanoparticles for data storage and a tunnelling process in the high conductance state. Such hybrid bio–inorganic nanostructures show promise for applications in future nanoelectronics.

Nanostructured biomaterials represent an ideal system for use in biological detection due to their unique selectivity[1,2]. Important developments have been made in the synthesis of bionanostructures with nanocrystals, including protein-shelled viruses modified by metallic[3–6] or semiconducting nanoparticles[7,8]. Significant advances have also been reported in the application of nanocrystal structures on DNA molecules[9–11] for detection of a variety of moieties[12]. However, organizing ordered inorganic nanoparticles by using soft materials as templates is essential for constructing electronic devices with new functionalities[13]. Such functionalities have been realized in biomolecule-assisted assembly bridging nanoscale electrical circuits[14]. However, there are few examples of electronic devices being directly fabricated from biomaterials owing to a lack of charge transport through them[15,16]. We report a new memory-effect function in the hybrid system composed of tobacco mosaic virus (TMV) conjugated with platinum nanoparticles (TMV–Pt). The augmentation of electrical conductivity in this TMV–Pt nanocomposite modifies its properties and makes it a suitable candidate for electronic applications. Such systems show electrical bistability depending on the voltage-controlled conductance states. The important features of this bistability include non-volatility, low operating voltage and large on/off ratio. In a previous work, we demonstrated this type of switching in devices based on metal nanoparticles linked with a conducting polymer[17]. This switching behaviour is now extended to biological materials such as TMV. The dimensions of this TMV–Pt device can be reduced and the system can be integrated using nanofabrication techniques.

RESULTS

MICROSCOPY CHARACTERIZATION

The TMV is a positive-sense single-stranded RNA plant virus composed of 2,130 identical coat proteins. TMV is placed in Group IV under the Baltimore classification system for viruses because the genome encapsulated within the TMV coat protein is a positive-sense single-stranded RNA. Positive-sense RNA can act as viral messenger RNA in which the viral RNA itself is infectious (that is, it can be directly translated by the host cell). The rigid virion is a 300-nm-long tube with 18-nm outer and 4-nm inner diameters. The chemical and physical stability of TMV has been studied under different conditions, including temperature, pH and so on, proving the robustness of the TMV structure[18]. Although there are several strains and mutants of TMV, wild-type TMV-U1 was chosen as the nanotemplate for synthesis. The conjugation of nanoparticles with TMV was carried out by using a platinum ion solution for electroless deposition[3–6]. The metal ions are able to bind with specific functional groups on the protein surface of the virus[19]. The Pt nanoparticles (NPs) are quite uniformly distributed on the virus surface (Fig. 1) and have sizes ranging from 7 to 15 nm, with an average size of ~10 nm.

The core-level X-ray photoelectron spectra (XPS) of Pt 4*f*, C 1*s*, N 1*s* and O 1*s* are presented in Fig. 2. We observed two distinct chemical components from Pt $4f_{7/2}$ at 71.8 and 73.4 eV. The same result was obtained for Pt $4f_{5/2}$ at 75 and 77 eV, as shown in Fig. 2a. The high binding-energy peak is attributed to positively charged Pt particles bonded with TMV coat proteins. The low binding-energy peak originates from the Pt metal core.

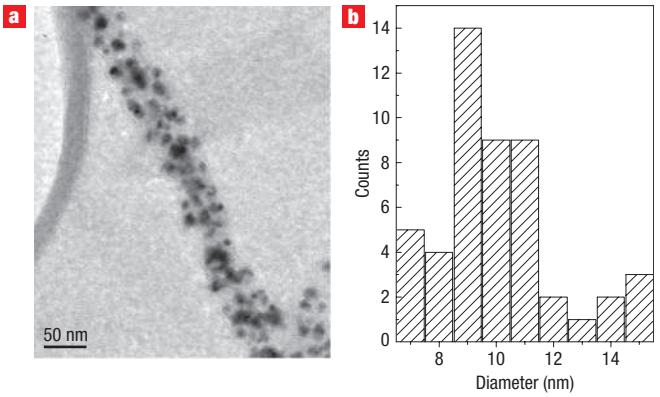

Figure 1 Transmission electron microscope (TEM) image of TMV–Pt conjugate and size distribution of the Pt nanoparticles. a, TEM image of TMV nanowire conjugated with Pt nanoparticles. The Pt nanoparticles have an average size of ~10 nm and are uniformly attached at the surface of the virus wire. **b**, Histogram showing the size distribution of the nanoparticles, measuring between 7 and 15 nm.

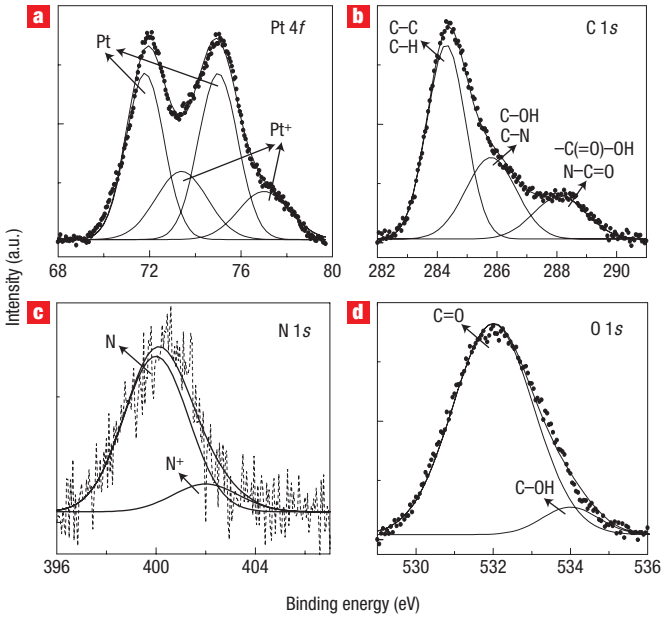

Figure 2 XPS spectra of hybrid bio-inorganic TMV–Pt composites. a, The Pt 4*f* core-level spectrum shows the Pt metal core and a high-binding-energy component attributed to partially positively charged Pt^{+}. **b**, The core-level spectra of C 1*s* are resolved into components of hydrocarbon (C–C, C–H), carbon–nitrogen (C–N), hydroxyl groups (C–OH), carboxylate (–C(=O)–OH) and amide carbon (N–C=O). **c**, N 1*s* and **d**, O 1*s* spectra are also resolved into neutral N, protonated N, and C=O, C–OH, respectively.

The C 1*s* peak in Fig. 2b can be resolved into three main components. The hydrocarbon (C–C, C–H) is located at 284.5 eV. Carbon bound to nitrogen (C–N) and hydroxyl groups (C–OH) are located at 285.8 eV. The binding energy of carbon in the hydroxyl group in TMV–Pt, compared with a system with no Pt, is shifted by ~0.5 eV to a lower energy, suggesting the bonding of Pt^{+} to the C–OH group. Carboxylate (–C(=O)–OH) and amide carbon (N–C=O) are located at 288.1 eV. It has been previously reported that the 288.1 eV of the C 1*s* spectrum accounts for the carboxylate carbon from the metal-particle-bound tyrosine[20]. There are two main components in the N 1*s* level, centred at 400 and 402 eV in Fig. 2c, where the high binding-energy peak suggests the protonated amino group. Two distinct peaks at 532 and 534 eV in the O 1*s* spectrum represent the incorporation of C=O and C–OH components, respectively[21]. These qualitative components obtained by curve-fitting are consistent with the reported values[20–22]. Thus, the outer surface of TMV, containing mainly hydroxyl groups and carboxyl termini[6], provides the primary binding sites for Pt NPs as resolved by XPS. A qualitatively componential analysis of TMV–Pt is also presented.

This TMV–Pt composite system exhibits unique conductance-switching behaviour, and can therefore be used in the first electronic biomemory device. The electrical switching effect has been observed in nanoparticles incorporated into polymer/organic thin films[23,24]. These films use the nanoparticles as charge traps or to create a molecular-doped polymer so that the film conductivity can be tuned. As yet, electronic transport at the interface of the biomaterials and the nanoparticles has not been explored. This system based on TMV–Pt provides a unique insight into using the combination of virus and nanoparticles for memory effect. These devices were fabricated through a solution process with a hybrid bio-inorganic composite layer in a polyvinyl alcohol (PVA) matrix sandwiched between two electrodes. Details of the material and device fabrication procedure are provided in the Methods section.

CURRENT–VOLTAGE CHARACTERISTICS

The inset in Fig. 3 is a schematic of the device structure, consisting of dispersed TMV–Pt nanowires in a PVA matrix sandwiched between two Al electrodes. The nonlinear current (I)–voltage (V) characteristic (Fig. 3) arises from the bistable electrical behaviour of the TMV–Pt device. In the first scan, the current gradually increases as the voltage is increased to 3 V. An abrupt increase in the current by more than three orders of magnitude (from 10^{-8} A to 10^{-5} A) occurs once a turn-on bias (3.1 V) is reached. A second scan is performed on the device to ensure the stability of the high conductance state (10^{-5} A). We normally term the low conductance state (10^{-9} A) and the high conductance state (10^{-6} A) as the OFF and ON states, respectively. The OFF and ON states can also be denoted by '0' and '1' in practical data storage terms. The ON state can be switched back to the OFF state by applying a third backward scan. From 0 to −5 V, the current drops from 10^{-5} A to 10^{-7} A at a turn-off bias of −2.4 V. The device is stable in the OFF state until a forward bias larger than 3 V is applied, which turns it to the ON state once again. Conductance switching is not observed in control devices using only TMV or only PVA, fabricated with the same concentration and thickness. The function of PVA is to provide a polymer matrix for TMV–Pt and to prevent electrical shortages.

Devices containing only Pt NPs were also fabricated to test for bistability behaviour. The Pt NPs were synthesized by the same method as used for TMV–Pt, and were dispersed in the PVA matrix with similar concentrations. The nanostructure image of the Pt NPs shows a particle size between 6 and 18 nm (see Supplementary Information). The I–V characteristic shows a high conductance without switching effect, although a slight hysterisis behaviour is observed. This device shows no erasable capability, which is necessary for digital memories, and the high conductance cannot return to the low conductance state. It is therefore obvious that the hybrid bio-inorganic TMV–Pt nanostructure is required to provide genuine rewritable

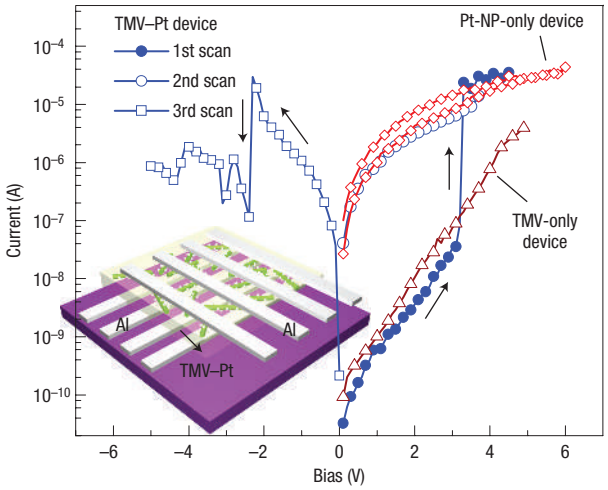

Figure 3 Typical room temperature *I–V* characteristics of the TMV–Pt device. The first bias scan (filled circles) shows the device switch to the ON state at 3.1 V and stablize in the ON state, as confirmed by the second scan (open circles). A reverse scan (squares) indicates that the device turns back to the OFF state at −2.4 V. The *I–V* curves of TMV-only (triangles) and Pt-NP-only (diamonds) devices show no conductance switching. The inset shows a schematic of the device structure with an active layer of dispersed TMV–Pt nanowires.

non-volatile states for a 2-bit memory application. These non-volatile bistable states represent an exciting discovery, where electronic functionality has been introduced for the first time in protein-shelled viruses conjugated with nanoparticles.

CONDUCTION MECHANISM OF ON AND OFF STATES

The conduction mechanism of the device in the ON and OFF states can be understood by carrying out temperature-dependent measurements and fitting different mechanisms. The current in the OFF state is due to thermionic emission involving thermally activated charge injection from the electrodes to the TMV–Pt wires. The currents in the OFF state show a linear relation for $\ln(I/T^2)$ versus $1/T$ (Fig. 4a) and also for $\ln(I)$ versus $V^{1/2}$ (Fig. 4b). This OFF-state current is essentially considered to be leakage current occurring before the switching transition occurs. The current in the ON state measured at different temperatures is shown in Fig. 4c. No obvious change is observed between room temperature and 130 K, indicating a tunnelling conduction process. Thus we fitted the current in the ON state using a Fowler–Nordheim tunnelling model. At higher voltages (>0.8 V), a linear relation of $\ln(I/V^2)$ versus $1/V$ is observed (Fig. 4d). Therefore, in the ON state, the conduction mechanism is no longer thermionic injection as in the OFF state, but charge tunnelling.

CONDUCTIVE ATOMIC FORCE MICROSCOPY (CAFM) MEASUREMENT

The CAFM measurement is used to show conductance switching in a single TMV–Pt wire. A morphology image (Fig. 4e) shows the virus, which has the dimensions ~300 nm (length), 32 nm (width) and 8 nm (height). These dimensions are in conformity with observations from transmission electron microscopy (TEM) where the TMV wire is coated with Pt nanoparticles, making the total diameter about 30 nm. Note that some nanoparticle clusters are attached at each node of the TMV wire. First the TMV–Pt composite is located on the substrate surface by the tapping-mode AFM. Then a CAFM tip (contact mode) is biased from 0 to 6 V, while located on top of the TMV–Pt. The current collected from the substrate shows switching by over three orders of magnitude at a switch-on bias of ~4 V, whereas the TMV-only sample shows no conductance switching (Fig. 4f). This proves that each TMV–Pt nanowire is responsible for switching and memory effects.

SWITCHING CYCLES

Figure 5 shows the switching cycles of the TMV–Pt memory device, which were analysed by an HP 4155B with an installed IBasic program. The 'write' pulse of 2.5 V and 'erase' pulse of −1.5 V, both with a time width of 10^{-4} s, were used to turn the device ON and OFF, respectively. Between the two programming pulses, a 'read' pulse of 0.6 V was used to measure the current level of the device and determine its conductance state. The device can be programmed for roughly 400 cycles with an ON/OFF ratio of between 100 and 1,000. However, with an increasing number of cycles, we found that it became more difficult to return to the OFF state from the ON state. The failure of the device can be rationalized from the degradation of the TMV–nanoparticle interface through Joule heating during operation of the device. There remains a lot of room for improving the performance of the device using more refined engineering techniques.

RETENTION TIME

Another substantial factor that determines the performance of the TMV–Pt memory device is the retention time. Figure 6a shows the data retention of the device measured by applying a voltage of 1 V every 10 s, at various temperatures. The effect of temperature on the memory decay sheds light on the charge storage mechanism and on the potential for commercialization[25]. The current in the ON state decays faster at the highest temperature of 380 K, suggesting a temperature-dependent rate of charge loss. The probability of charge loss is proportional to the temperature and inversely proportional to the effective barrier height of the charge trap as expressed by $f \propto \exp(-\Delta E/kT)$ where ΔE is the activation energy of the charge trap, k is Boltzmann's constant and T is absolute temperature. The trap sites are located on the nanoparticles present on the TMV backbone within the insulating PVA matrix. The protein coat on the TMV surface is likely to be this effective energy barrier because of its relatively stable structure. The resulting charge retention is inversely proportional to the probability of charge loss, described by the equation $\tau \propto \tau_0 \exp(\Delta E/kT)$, where τ is the retention time, defined as the time for the current in the ON state to decay to 1% of its original value and τ_0 is a constant. The activation energy of the charge trap determined from the slope of the Arrhenius plot (Fig. 6b) is 0.15 ± 0.03 eV. The thermal energy at 380 K is ~0.03 eV, so the magnitude of decay of charge retention and current fluctuation are larger than those at low temperatures. The activation energy is close to the charging energy of nanoparticles with similar particle sizes[26]. The coulomb charging energy follows the relation $E = e^2/2C$, where the capacitance C relates to the morphology of the nanoparticle in the device configuration. This charging energy is the energy that needs to be overcome for charge trapping to occur. Other examples such as monolayer-protected gold nanoparticles also report similar charging energy[27,28] and charge trap behaviour[29]. Our charge-trapping-based device differs distinctly from non-charge-based resistance change memory[30], where conductivity and retention have very weak temperature dependence due to the stable molecular conformation. It is therefore clear that in the present case, device performance depends on the charge-trapping ability of nanoparticles from the TMV–Pt sandwiched in the insulating matrix. A schematic energy diagram (inset in Fig. 6b) illustrates the trap energy in the nanoparticles.

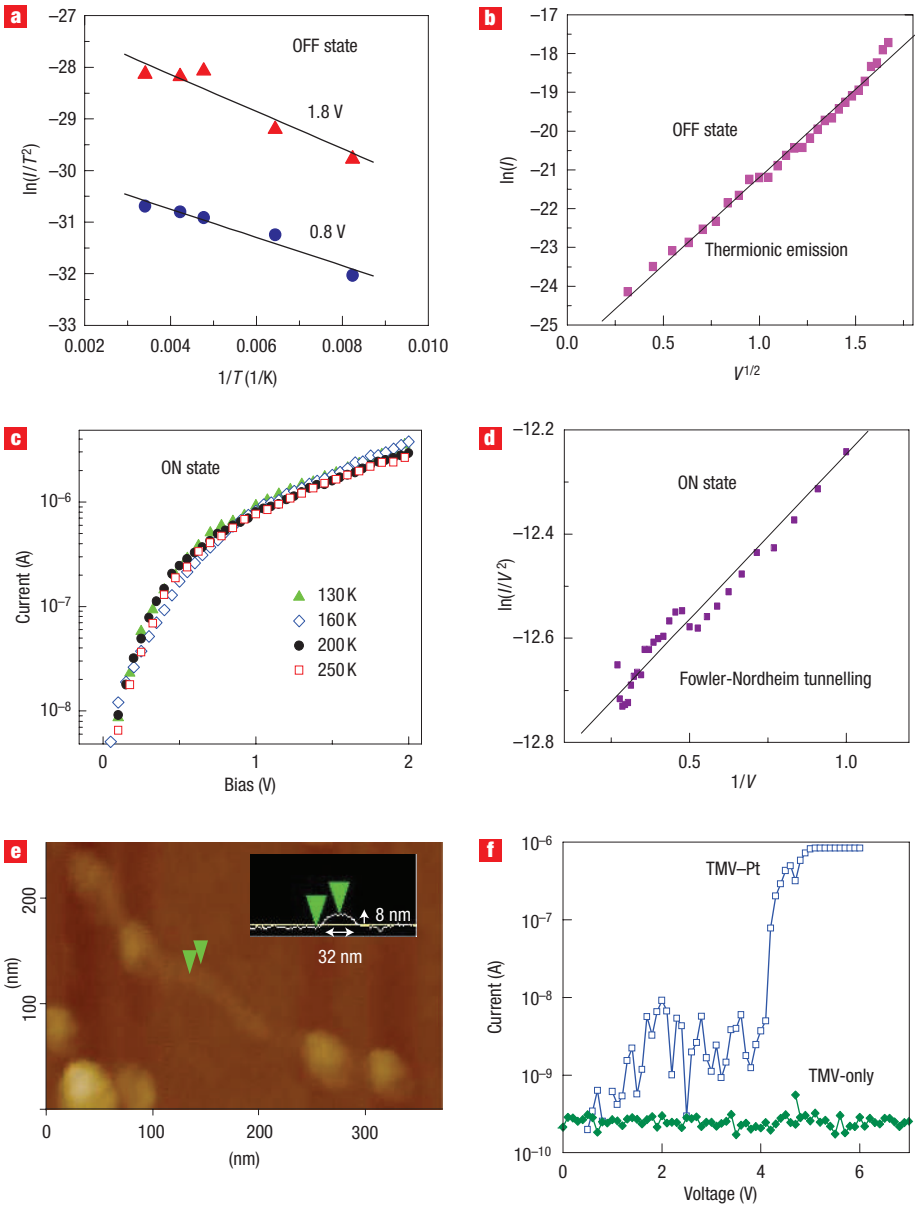

Figure 4 The conduction mechanism and conductive atomic force microscope measurements. a, The temperature-dependent OFF current shows a linear relation for $\ln(I/T^2)$ versus $1/T$ at selected voltages. **b**, The currents in the OFF state also exhibit a linear relation for $\ln(I)$ versus $V^{1/2}$. The currents in the OFF state were attributed to thermionic emission. **c**, The currents in the ON state were measured at different temperatures with no obvious changes. **d**, The currents in the ON state were attributed to Fowler–Nordheim tunnelling at a higher voltage regime (>0.8 V). **e**, The morphology image shows a single TMV–Pt wire. The sample is prepared by drop-casting TMV–Pt wires on the Si substrate. **f**, When a voltage scan from 0 to 6 V is applied, conductance switching is observed on the TMV–Pt, but the TMV-only configuration shows no switching transition.

DISCUSSION

From the TEM and AFM images of the TMV–Pt nanostructure, the diameter of the nanowires is about 30 nm, with an average particle size of 10 nm and an average density of roughly 16 particles per virus. With the current crossbar configuration, there are about 1–2 parallel TMV–Pt nanowires embedded in the thin film between the two electrodes. A comparative study on the device with only Pt NPs shows the conduction current close to the ON state, whereas the TMV-only devices show the current in the OFF state. These NP-only or TMV-only devices do not have the memory effect. The unique memory effect is established by the combination of TMV and Pt NPs. The function of the TMV is not just to provide a backbone for the organization of discrete nanoparticles. Indeed, the TMV consists of an RNA core with rich aromatic rings, such as guanine, which can behave as charge donors. The ionization energy of guanine is 7.85 eV in the gas phase[31], which is comparable to organic donors such as anthracene (7.4 eV), and thus guanine can behave as a charge donor with its aromatic ring. The proteins on the surface of the TMV virus, which separates the RNA and Pt NP, act as the energy barrier. The mechanism of our memory device, including the

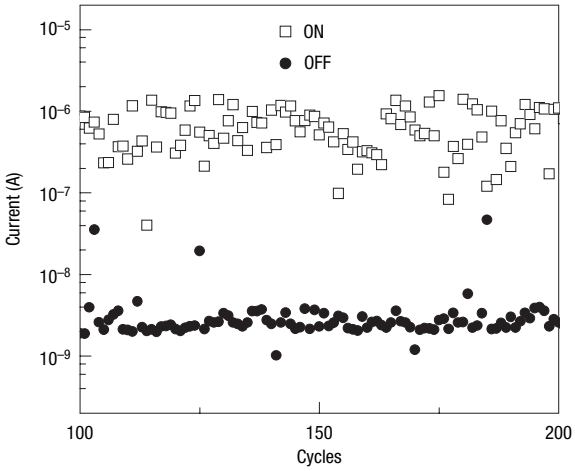

Figure 5 Switching cycles of the TMV–Pt device. The currents during the cycles are shown for the ON or OFF states. Write, erase and read voltages of 2.5, −1.5 and 0.6 V, respectively, are used to program this device.

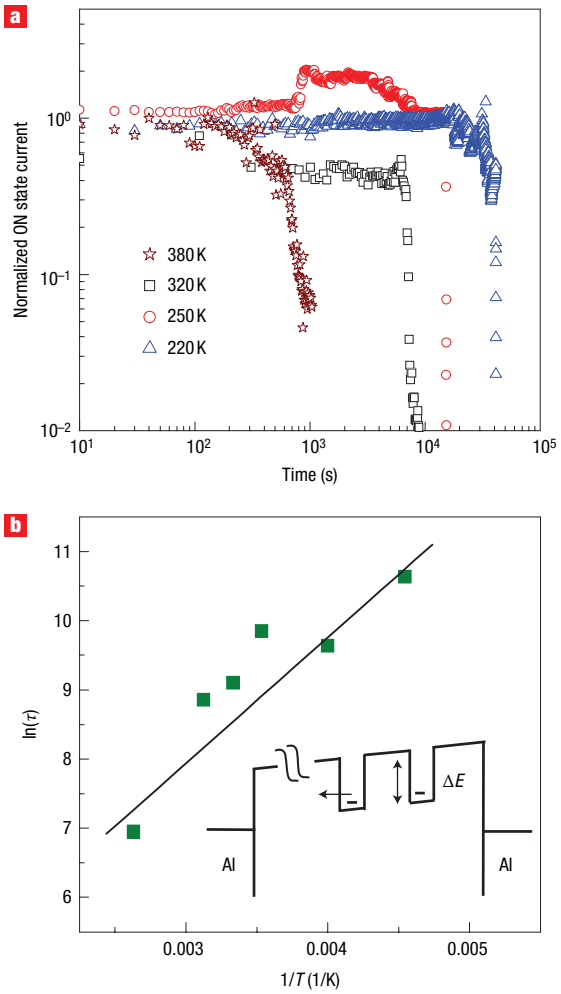

Figure 6 Temperature-dependent retention time. a, The data retentions were measured at different temperatures, showing the charge retention time as a function of temperature. **b**, The activation energy of the charge trap is determined from the slope of the Arrhenius plot of the charge retention time versus inverse temperature. A schematic energy diagram of the charge trap activation energy (ΔE) is shown in the inset. The symbol '–' is used to denote the trapped charges.

sudden jump of the current in the I–V scan, is likely due to charge transfer from the RNA to the Pt NPs under the high electric field, subsequently changing the conductivity of the material system[23]. Once the charge is being transferred, it will be trapped in the nanoparticles and stabilized by the coat proteins. As this is an electrical field effect, when sufficient numbers of sites are established, a sudden jump of current accompanying the charge tunnelling through the nanoparticles is observed. The activation energy of charge trapping and the temperature-dependent charge retention are strong evidence for the trapping behaviour of nanoparticles. After a couple of charges are de-trapped from the nanoparticles, and return to the RNA, the conductivity of the material system drops to the OFF state. These interactions between the RNA and protein in the TMV with the Pt NPs augment the write and erase processes in the memory device, but the switching is not observed in TMV- and Pt NP-only devices. The TMV therefore plays a role in not only organizing the small-size Pt NPs, but also acting as charge donor and stabilizing the charges in creating a repeatable memory effect in the TMV–Pt devices.

Despite successfully demonstrating a memory effect in TMV–Pt, several issues regarding the performance of the memory devices should be addressed. The metal nanoparticles demonstrate a size-dependent electron relaxation process[32], allowing trapped charges to be perturbed by thermal energy. Therefore, the retention stability and cycling endurance of the device could be further improved by introducing smaller-sized or other types of nanoparticles. In addition, different mutants or chemically modified viruses[33] may enhance or reduce the dipole interaction between the nanoparticles and viruses. The resulting change in conductance states in the TMV–Pt device may provide different electrical signals for other biological applications.

In conclusion, an electronic bistable device based on TMV–Pt nanowires has been reported with unique non-volatile memory properties. One-dimensional TMV biomolecules offer an ideal template for nucleation and growth of Pt NPs of size ~10 nm. A qualitative chemical component analysis of TMV–Pt was resolved by XPS. The memory devices were fabricated through a simple solution process with this hybrid bio-inorganic composite layer sandwiched between two electrodes. Basic memory operations, such as operating voltages, data retention and cycle ability are presented. Charge transfer and charge traps in nanoparticles are responsible for the conductance switching behaviour and the memory effect. The concept of conjugating nanoparticles with biomolecules opens up new possibilities for making functional electronic devices using biomaterial systems.

METHODS

MATERIALS SYNTHESIS

The TMV virus was first suspended in deionized water to a concentration of ~1 mg ml^{-1}, followed by the addition of 1-mM potassium tetrachloroplatinate (K_2PtCl_4) with a volume ratio 65:1 (K_2PtCl_4:TMV). The mixture was kept at room temperature for approximately 3 h to obtain virus capsid activated by the Pt ions. Then, 1 μl 10-mM dimethylamine borane was added to provide a reduction bath for Pt ions to form Pt clusters on the surface of the virus particles. The sample was incubated at 27 °C for 2 h. The final product was washed by centrifugal filtration, several times, to remove unreacted reagents.

MICROSCOPY CHARACTERIZATION

The TEM images were obtained with a Philips CM300 under 100 kV. The samples were prepared by drop-casting the nanowire solutions on lacy carbon copper grids. XPS was used to resolve the chemical components of the TMV–Pt using an OMICRON Multiprobe with a monochromatic Al Kα radiation (12,563.6 eV, 300 W) source. The base pressure of the analysis chamber was smaller than 10^{-9} torr. The samples were prepared by drop-casting TMV–Pt nanowires on Au-coated Si substrates attached to a stainless-steel holder. The resolution of the measurement was about 0.1 eV. For all spectra, a linear constant background was subtracted and peak fitting was performed using a symmetric Gauss–Lorentz function. No apparent binding energy shift was observed for Au 4*f* peaks (84 and 87.7 eV) from the substrate, indicating no charging effect in the sample. The CAFM was measured using a Multimode AFM (Nanoscope IIIa, Veeco Instruments) with conductive AFM tips (NSC11/Ti–Pt, titanium–platinum-coated Si tip with a radius of $<$30 nm). The sample was prepared by drop-casting TMV–Pt wires on the Si substrate. The tip is biased and scanned on the sample in contact mode and the current is collected from the substrate.

DEVICE FABRICATION

We fabricated the TMV–Pt devices by the following simple process. The bottom Al electrodes were deposited on a bare glass substrate by thermal evaporation, in a chamber with a background pressure of 5×10^{-6} torr. An aqueous solution with concentrations of ~0.1 wt% TMV–Pt nanowires in 1.2 wt% PVA ($M_w = 90{,}000$) was used. A thin film was then spin-coated onto the substrate, where the virus wires were dispersed in an electrically insulating PVA matrix. The thicknesses of the Al electrode and the thin film, as determined by Dektak profilometer, were 70 and 60 nm, respectively. The device covered an active area of 0.04 mm^2. Current–voltage, data cycle and retention characteristics were measured using the HP 4155B Semiconductor Parameter Analyser.

Received 5 June 2006; accepted 30 August 2006; published 4 October 2006.

References

1. Alivisatos, P. The use of nanocrystals in biological detection. *Nature Biotechnol.* **22,** 47–52 (2004).
2. Zheng, G., Patolsky, F., Cui, Y., Wang, W. U. & Lieber, C. M. Multiplexed electrical detection of cancer markers with nanowire sensor arrays. *Nature Biotechnol.* **23,** 1294–1303 (2005).
3. Dujardin, E., Peet, C., Stubbs, G., Culver, J. N. & Mann, S. Organization of metallic nanoparticles using tobacco mosaic virus templates. *Nano Lett.* **3,** 413–417 (2003).
4. Knez, M. *et al.* Spatially selective nucleation of metal clusters on the tobacco mosaic virus. *Adv. Funct. Mater.* **14,** 116–124 (2004).
5. Behrens, S., Wu, J., Habicht, W. & Unger, E. Silver nanoparticle and nanowire formation by microtubule templates. *Chem. Mater.* **16,** 3085–3090 (2004).
6. Richter, J. *et al.* Nanoscale palladium metallization of DNA. *Adv. Mater.* **12,** 507–510 (2000).
7. Mao, C. *et al.* Virus-based toolkit for the directed synthesis of magnetic and semiconducting nanowires. *Science* **303,** 213–217 (2004).
8. Shenton, W. *et al.* Inorganic–organic nanotube composites from template mineralization of tobacco mosaic virus. *Adv. Mater.* **11,** 253–256 (1999).
9. Belcher, A. M. *et al.* Control of crystal phase switching and orientation by soluble mollusc-shell proteins. *Nature* **381,** 56–58 (1996).
10. Mirkin, C. A., Letsinger, R. L., Mucic, R. C. & Storhoff, J. J. A DNA-based method for rationally assembling nanoparticles into macroscopic materials. *Nature* **382,** 607–609 (1996).
11. Mertig, M. *et al.* DNA as a selective metallization template. *Nano Lett.* **2,** 841–844 (2002).
12. Karhanek, M. *et al.* Single DNA molecule detection using nanopipettes and nanoparticles. *Nano Lett.* **5,** 403–407 (2005).
13. Lee, S. W., Mao, C., Flynn, C. E. & Belcher, A. M. Ordering of quantum dots using genetically engineered viruses. *Science* **296,** 892–895 (2002).
14. Chung, S. W. *et al.* Top-down meets bottom-up: dip-pen nanolithography and DNA-directed assembly of nanoscale electrical circuits. *Small* **1,** 64–69 (2005).
15. Weetall, H. H. Innovations in biomolecular electronics. *Biotechnol. Prog.* **15,** 963 (1999).
16. Maruccio, G. *et al.* Nano-scaled biomolecular field-effect transistors: prototypes and evaluations. *Electroanalysis* **16,** 1853–1862 (2004).
17. Tseng, R. J. *et al.* Polyaniline nanofiber/gold nanoparticle nonvolatile memory. *Nano Lett.* **5,** 1077–1080 (2005).
18. Knez, M. *et al.* Biotemplate synthesis of 3-nm nickel and cobalt nanowires. *Nano Lett.* **3,** 1079–1082 (2003).
19. Schlick, T. L., Ding, Z., Kovacs, E. W. & Francis, M. B. Dual-surface modification of the tobacco mosaic virus. *J. Am. Chem. Soc.* **127,** 3718–3723 (2005).
20. Selvakannan, P. R. *et al.* Synthesis of aqueous Au core–Ag shell nanoparticles using tyrosine as a pH-dependent reducing agent and assembling phase-transferred silver nanoparticles at the air–water interface. *Langmuir* **20,** 7825–7836 (2004).
21. May, C. J., Canavan, H. E. & Castner, D. G. Quantitative X-ray photoelectron spectroscopy and time-of-flight secondary ion mass spectroscopy characterization of the components in DNA. *Anal. Chem.* **76,** 1114–1122 (2004).
22. Petrovykh, D. Y., Kimura-Suda, H., Whitman, L. J. & Tarlov, M. J. Quantitative analysis and characterization of DNA immobilized on gold. *J. Am. Chem. Soc.* **125,** 5219–5226 (2003).
23. Ouyang, J. *et al.* Programmable polymer thin film and nonvolatile memory device. *Nature Mater.* **3,** 918–922 (2004).
24. Ma, L. P., Liu, J. & Yang, Y. Organic electrical bistable devices and rewritable memory cells. *Appl. Phys. Lett.* **80,** 2997–2999 (2002).
25. Gerstner, E. G. & McKenzie, D. R. Nonvolatile memory effects in nitrogen doped tetrahedral amorphous carbon thin films. *J. Appl. Phys.* **84,** 5647–5651 (1998).
26. Saitoh, M., Takahashi, N., Ishikuro, H. & Hiramoto, T. Large electron addition energy above 250 meV in a silicon quantum dot in a single-electron transistor. *Jpn J. Appl. Phys.* **40,** 2010–2012 (2001).
27. Chen, S., Murray, R. W. & Feldberg, S. W. Quantized capacitance charging of monolayer-protected Au clusters. *J. Phys. Chem. B* **102,** 9898–9907 (1998).
28. Ouyang, J. *et al.* Organic memory device fabricated through solution processing. *Proc. IEEE* **93,** 1287–1296 (2005).
29. Tseng, R. J. *et al.* Nanoparticle-induced negative differential resistance and memory effect in polymer bistable light-emitting device. *Appl. Phys. Lett.* **88,** 123506 (2006).
30. Cai, L. *et al.* Reversible bistable switching in nanoscale thiol-substituted oligoaniline molecular junctions. *Nano Lett.* **5,** 2365–2372 (2005).
31. Chemistry WebBook of the National Institute of Standards and Technology, 22nd August, 2006. http://webbook.nist.giv/chemistry.
32. Hamanaka, Y. *et al.* Ultrafast electron relaxation via breathing vibration of gold nanoparticles embedded in a dielectric medium. *Phys. Rev. B* **63,** 104302 (2001).
33. Raja, K. S. *et al.* Hybrid virus–polymer materials. 1. Synthesis and properties of PEG-decorated cowpea mosaic virus. *Biomacromol.* **4,** 472–476 (2003).

Acknowledgements

This research work was supported by the Microelectronics Advanced Research Corporation (MARCO) Focus Center on Functional Engineered Nano Architectonics (FENA) at the University of California, Los Angeles, and the University of California, Riverside, and the Air Force Office of Scientific Research. We acknowledge assistance from Paichun Chang, Zhiyong Fan and Jia Grace Lu on the CAFM measurements.
Correspondence and request for materials should be addressed to Y.Y. and C.S.O.
Supplementary Information accompanies this paper on www.nature.com/naturenanotechnology.

Author contributions

R.J.T. and C.T. designed the experiments. R.J.T. performed memory device fabrication, XPS characterization, CAFM, and electrical measurements. C.T. performed material synthesis, TEM, SEM images and CAFM study. L.P.M. provided feedback and the model for the device mechanism. J.O. provided suggestions on the experiments. C.S.O. and Y.Y. conceptualized and directed the research project. All authors discussed the results and commented on the manuscript.

Competing financial interests

The authors declare that they have no competing financial interests.